Deterministic Tuning of Single Mixed (Helical) Dislocations in Core-Shell van der Waals Nanowires

Peter Sutter,[1,*] Raymond R. Unocic,[2] and Eli Sutter[3,*]

[1]Department of Electrical & Computer Engineering, University of Nebraska-Lincoln, Lincoln, Nebraska 68588, United States

[2]Center for Nanophase Materials Sciences, Oak Ridge National Laboratory, Oak Ridge, TN 37831, United States

[3]Department of Mechanical & Materials Engineering, University of Nebraska-Lincoln, Lincoln, NE 68588, United States

[*]Corresponding authors, e-mail: psutter@unl.edu, esutter@unl.edu

Keywords: Linear defects, dislocations, layered crystals, core-shell heterostructures

Abstract

Linear defects (dislocations) not only govern the mechanical properties of crystalline solids, but they can produce distinct electronic, thermal, and topological effects. Accessing this functionality requires control over the placement and geometry of single dislocations, embedded in a small host volume to maximize emerging effects. Here we identify a synthetic route for rational dislocation placement and tuning in van der Waals nanowires, where the layered crystal limits the possible defect configurations and the nanowire architecture puts single dislocations in close proximity to the entire host volume. While homogeneous layered nanowires host single screw dislocations, synthesis of radial nanowire heterostructures (here exemplified by GeS-$Ge_{1-x}Sn_xS$ monochalcogenide core-shell nanowires) transforms the defect into a mixed (helical) dislocation whose edge/screw ratio is tunable *via* the core-shell lattice mismatch. The ability to design nanomaterials with control over individual mixed dislocations paves the way for identifying the functional properties of dislocations and for harnessing them in technology.

1. Introduction

Defects that break the perfect lattice periodicity are innate to all crystalline materials and often dictate their properties. Linear defects (dislocations) and their ability to move under applied forces define mechanical properties including ductility, hardness, and yield strength. Since the emergence of information technology, defects have been considered detrimental to the functional properties of electronic materials. Point defects such as vacancies, interstitials, antisites, and defect complexes introduce states within the bandgap[1] and act as scattering centers that reduce the carrier mobility.[2] Dislocations can give rise to deep-level trap states that promote nonradiative recombination,[3-5] or cause increased leakage and premature breakdown in devices.[6]

In many instances, however, defects can be beneficial to electronic materials and devices by providing access to functionality beyond that of perfect crystals. A classic example is substitutional doping of semiconductors,[7] which enables tuning the free carrier concentration over many orders of magnitude. More recently, point defects such as color centers and impurity-vacancy complexes (*e.g.*, nitrogen-vacancy centers in diamond)[8] have become key components for emerging quantum technologies as single photon emitters and spin qubits.[9]

Similar to point defects, linear defects promise useful functional properties by breaking the lattice periodicity, introducing new electronic states, spin textures, or topological characteristics. The two pure forms, edge and screw dislocations, are characterized by a lattice distortion (measured by the Burgers vector, **b**) perpendicular and parallel to the line direction, respectively. Screw dislocations play a crucial role in a wide range of natural and technological processes. In biology, screw dislocations provide one of the fundamental mechanisms underlying cellular organization;[10] helicoidal structures connecting membrane sheets are essential for mass transport in the endoplasmic reticulum of eukaryotic cells.[11] Spiral growth around screw dislocations

facilitates crystal growth by enabling continuous materials incorporation without nucleation.[12] Screw dislocations in layered crystals provide avenues for synthesizing van der Waals stacks with controlled interlayer twist.[13] Predicted electronic properties include dislocation spin-orbit coupling generating highly coherent spin textures,[14] Majorana bound states,[15] chiral anomalies with emergent magnetic flux in Dirac semimetals,[16, 17] probes of monopole charge in multi-Weyl semimetals,[18] and low-dimensional gapless modes in topological insulators.[19] Recent theoretical work has established a framework in which dislocations are treated as quantized quasiparticles (*'dislons'*) analogous to phonons.[20, 21] From this quantum theory of dislocations, additional functional properties have been predicted, including electronic effects such as an oscillatory electron energy near a dislocation core,[22] effects on phonons,[23] dislocation-induced superconductivity,[24] as well as topological and quantum phase transitions.

Fundamental studies and emerging technological uses of defect-derived functionality have so far focused almost exclusively on point defects. The judicious formation of line defects is complicated by the need to, along with the defect type, control the position and orientation within the host matrix. A second complication arises with promoting functionality due to extended defects embedded in a host crystal. At low concentration, small effects are expected due to an unfavorable ratio between defect and host volumes; at high concentration, controlling the properties (*e.g.*, type of dislocation, Burgers vector, *etc.*) becomes problematic. Conventional approaches fail to address these challenges. Mechanical deformation of bulk-like materials, for example, causes complex dislocation networks without control over defect type or distribution.[25] Top-down methods for creating dislocation arrays and subsequently isolating single defects in a limited host volume require complex crystal engineering and device fabrication.[26]

Here, we show that nanostructures of van der Waals crystals provide unprecedented opportunities for generating linear defects with tunable geometry, embedded in a small host volume so that the emerging functional properties are maximized. Layered crystals avoid the multiple symmetry-allowed dislocation configurations characteristic of 3D-crystalline materials, but are still able to realize both types of pure (as well as mixed) dislocations,[27, 28] unlike true 2D materials which can host only edge dislocations (Figure S1).[29] In particular, we demonstrate the ability to deterministically tune the ratio between the screw- and edge-character of single helical dislocations in van der Waals nanowires. Helical dislocations, mixed screw-edge dislocations that wind up into a helix around an axis defined by the line of an incipient screw dislocation,[30, 31] are ubiquitous in materials and have been observed in metals, metal alloys,[32] semiconductors,[33] and ionic crystals.[34] Helical dislocations are formed under conditions that involve a flow of vacancies or interstitials, *e.g.*, high-temperature treatments,[35] cooling,[36] quenching or irradiation of alloys,[37, 38] and doping of semiconductors.[39] Generated stochastically in bulk materials, however, the formation, geometry, and emerging properties of helical dislocations have proven difficult to understand or control.

2. Results and Discussion

Creating tunable single mixed dislocations in van der Waals nanowires

Figure 1 shows the synthetic approach for nanowires containing single helical dislocations with tunable ratio between edge- and screw character. Defect-free van der Waals nanowires obtained by vapor-liquid-solid (VLS) growth crystallize in a layered structure, as shown in Figure 1a. Often, such wires instead form as growth spirals around an axial screw dislocation (Figure 1b).[13] Given the ubiquitous presence of Au-rich catalyst particles at the nanowire tips, we conclude that the liquid VLS catalyst plays the role of mediating mass transport from the vapor

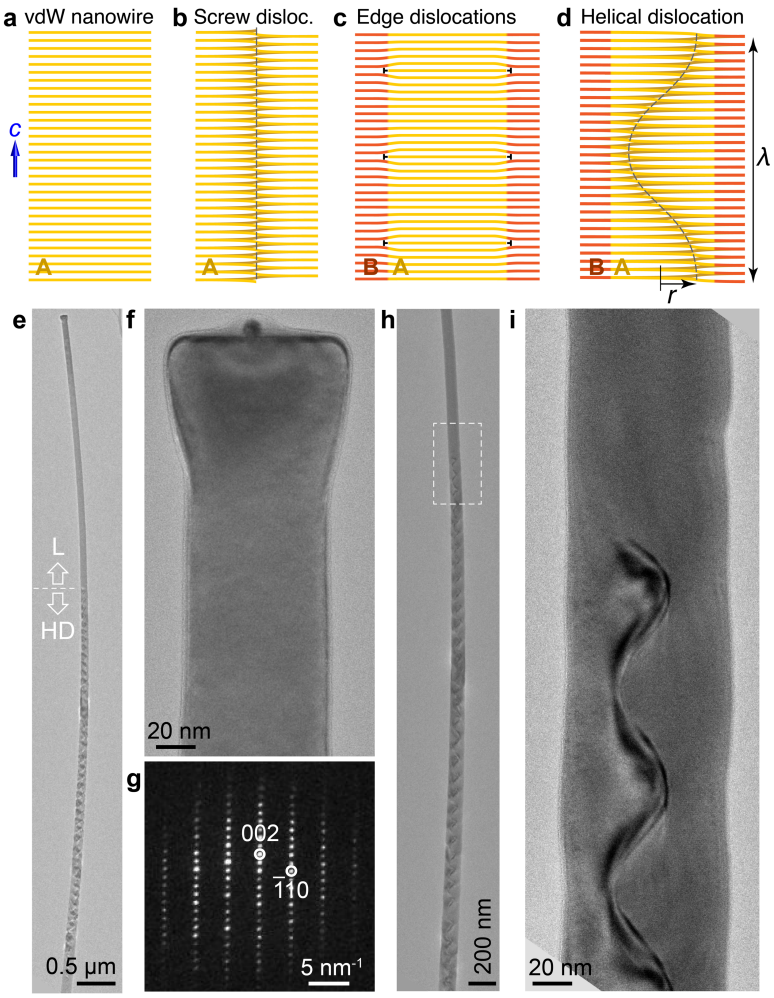

Figure 1. Synthesis of van der Waals nanowires with single mixed (helical) dislocations. a. Schematic cross-section of a layered nanowire. **b.–d.** Combining an axial screw dislocation (b.) with *c*-axis misfit (edge) dislocations in a core-shell structure (c.) produces van der Waals nanowires carrying single helical dislocations with mixed screw- and edge character (d.). **e.** TEM image of a nanowire showing a helical dislocation (HD) transitioning to a defect-free layered structure (L) near the tip. **f.** High-magnification TEM image of the nanowire close to the tip. **g.** Electron diffraction of the nanowire along the [110] zone axis, showing the *c*-direction of the crystal aligned with the symmetry axis of the wire. **h.** TEM image showing the transition between the nanowire with a helical screw dislocation and the non-dislocated segment near the tip. **i.** High-resolution TEM image of the helical dislocation near its exit point from the wire (area marked in f.).

phase to the nanowire growth front, while the open edge at the end of the spiral facilitates growth through continuous attachment without requiring any layer nucleation.[12, 40] Germanium sulfide (GeS) nanowires synthesized by VLS growth using different catalysts (Au,[41] Bi)[42] invariably contain axial screw dislocations over nearly the entire length, except close to the tip where the dislocations curve towards the surface and are ejected from the wires so that the final segment

consists of defect-free layered GeS (Figure S2). Prior work has linked this elimination of the dislocation from the wires to the injection of excess vacancies mediating climb of the dislocation to the surface at the onset of cooling near the end of the growth process;[41] the subsequent non-dislocated segment of the nanowire then grows through a regular VLS process.

Transforming such dislocated van der Waals nanowires into core-shell heterostructures holds the key to generating tunable mixed dislocations. Lattice mismatch in the axial direction (*i.e.*, in the *c*-axis (interlayer) spacing) between core and shell would normally be relaxed by edge dislocations (Figure 1c). In the presence of a screw dislocation, however, the two line defects can combine into a single mixed, helical dislocation (Figure 1d), whose screw/edge ratio is selectable *via* the core-shell mismatch, *i.e.*, the nominal spacing of core-shell misfit dislocations.

Van der Waals nanowire heterostructures realizing such tunable helical dislocations have been synthesized by a one-pot process employing simultaneous evaporation of two different precursors for group IV monochalcogenides, GeS and SnS. Adding SnS to the primary GeS precursor vapor up to moderate partial pressures (~20 mTorr, T_{SnS} = 620°C)[43] causes no detectable Sn incorporation into the nanowires but merely modifies the VLS growth, inducing morphology changes and switching the layering direction.[44] Further increasing the SnS vapor pressure (to 60-100 mTorr) at constant GeS vapor pressure (~250 mTorr, *i.e.*, ratio P_{SnS}:P_{GeS} > 1:4) switches the system back to VLS growth of layered nanowires with characteristic layer stacking (*i.e.*, *c*-axis) along the wire axis (Figure 1e-g). Similar to pure GeS nanowires (Figure S2), transmission electron microscopy (TEM) shows the presence of a dislocation, again except near the tip where the nanowires terminate in a few micrometer long defect-free segment (Figure 1h-i).[41] In the dislocated part, however, the characteristic straight line of the axial screw dislocation is replaced by a meandering, sinusoidal contrast that corresponds to the projection of

a helical dislocation viewed perpendicular to the axis of the helix (Figure 1d, i).[37, 45] Surveying many wires, we find that each nanowire supports one helical dislocation with a large number of turns, in some cases exceeding 120 turns over the length of the dislocated section.

Core-shell structure of van der Waals nanowires with helical dislocations

For the SnS-GeS system, the binary bulk phase diagram of the cations suggests essentially no solid solubility across the entire composition range (~1% Sn in Ge).[46] Applying Hume-Rothery

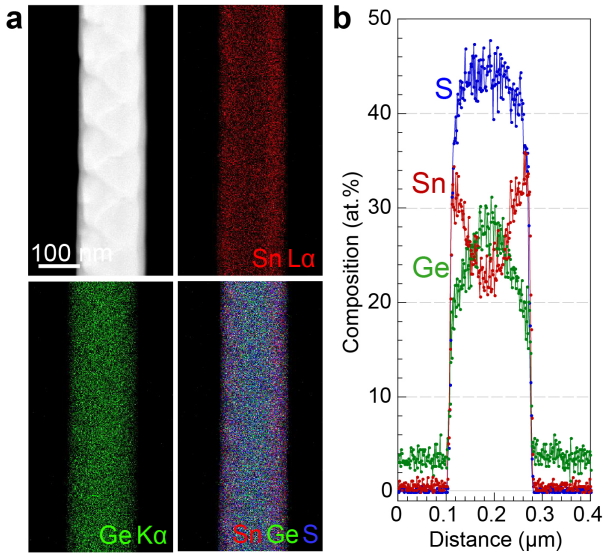

Figure 2. Composition of nanowires with helical dislocations. a. HAADF-STEM image along with tin, germanium, sulfur EDS elemental maps and a composite map. **b.** EDS line profile across the nanowire showing the Sn (red), Ge (green), and S (blue) distribution across the nanowire. The line profile represents an average over the length of the nanowire segment shown in a.

rules for the cations, this implies limited solid solubility for the isostructural and isoelectronic layered chalcogenides SnS and GeS. $Ge_{1-x}Sn_xS$ alloy nanoribbons indeed show phase separation of Ge- and Sn sulfides.[47] For $Ge_{1-x}Sn_xS$ nanowires, a similar phase separation causes the spontaneous formation of a core-shell structure. Energy dispersive X-ray spectroscopy (EDS) elemental maps show Ge, S, as well as Sn in the nanowires, *i.e.*, they consist of $Ge_{1-x}Sn_xS$ compounds. Composition maps (**Figure 2**a) and line profiles (Figure 2b) show uniform sulfur content, consistent with a constant anion to cation ratio across the monochalcogenide nanowires.

The relative abundance of Sn and Ge, on the other hand, varies between a Ge-rich core (28 at. % Ge; 22 at. % Sn) and a Sn-enriched near-surface region (15 at. % Ge; 35 at. % Sn). For inhomogeneous composition profiles – here a Sn-rich shell surrounding the cylindrical core – EDS analysis across the wires can only determine the composition of the Sn-rich $Ge_{0.3}Sn_{0.7}S$ near-surface region directly. When probing the core, the exciting electron beam also traverses the shell, which therefore contributes to the apparent core composition. The actual composition of the core can be estimated from the wire geometry and the EDS signals. The measured core diameter (90 nm) and shell thickness (40 nm) combined with the measured compositions translate to an actual core composition of ~40 at. % Ge, *i.e.*, the nanowire cores consist of a Ge-rich $Ge_{0.8}Sn_{0.2}S$ alloy. The phase separation and formation of a core-shell structure can occur either immediately upon incorporation from the molten VLS catalyst or shortly thereafter *via* solid-state diffusion. *In-situ* experiments in the TEM on nanowires with helical dislocations show no changes upon extended annealing of the wires at the growth temperature, supporting the conclusion that the separation into a GeS core and $Ge_{1-x}Sn_xS$ alloy shell, and thus the formation of the helical dislocation takes place during growth at high temperature rather than during cooling.

Eshelby twist in van der Waals nanowires with helical dislocations

Lattice spacings across the nanowires were determined using nanobeam electron diffraction linescans. Figure S3 shows parts of a sequence of 100 nanobeam diffraction patterns measured across a $Ge_{1-x}Sn_xS$ nanowire. The variation of the in-plane $(\bar{1}20)$ lattice spacing is consistent with the EDS measurements and shows the same trend across the nanowire, *i.e.*, a near-surface enrichment with SnS. However, the $(\bar{1}20)$ lattice constant generally remains close to that of the GeS-rich compound in the center. This suggests that the SnS-rich material at the surface is

strained to the lattice constant of the core, which is further supported by the uniformity of the structure and the absence of any defects (apart from the helical dislocation, Figure 1) expected when plastic relaxation between mismatched materials occurs.

Further diffraction analysis of the $Ge_{1-x}Sn_xS$ nanowires shows a twisted structure in the presence of helical dislocations. Nanobeam electron diffraction patterns recorded along the nanowires show the lattice rotation associated with Eshelby twist (Figure S3).[13, 40, 48] Eshelby predicted a twist $d\theta/dz = \mathbf{b}_z^s \left[\frac{1}{\pi R^2} - \frac{r_0^2}{\pi R^4}\right]$ due to a helical dislocation with (helix) radius r_0 in a nanowire with diameter $2R$, where $\mathbf{b}_z^s$ denotes the screw component of the Burgers vector of the dislocation.[49] Hence, the Eshelby twist is reduced relative to that of a straight screw dislocation, $d\theta/dz = \mathbf{b}_z/[\pi R^2]$ [50] (similar to hollow tubes,[51] see Figure S4). In a layered crystal, only screw dislocations with Burgers vectors equal to integer multiples of the layer spacing fulfill the crystallographic constraint of connecting adjacent layers. GeS nanowires with axial screw dislocations predominantly show Burgers vectors of multiples of the *c*-axis unit cell size (1.04 nm, comprising an A-B stacked bilayer; see Figure S5).[13, 42] For $Ge_{1-x}Sn_xS$ nanowires with helical dislocations, we frequently find half-unit cell Burgers vectors $\mathbf{b}_z^s$. Nanobeam diffraction of the wire shown in Figure S6 (diameter $2R$ = 124 nm, helix radius r_0 = 20 nm), for example, shows a twist of ~2.2°μm^{-1}. According to the Eshelby formalism, this twist corresponds to a helical dislocation with screw-component Burgers vector $\mathbf{b}_z^s = 0.52\,\mathrm{nm}$. The reduction in the screw component of the Burgers vector for helical dislocations can be understood by considering the formation process of the helical line. Starting from a straight screw dislocation, an edge component develops due to climb driven by the core-shell mismatch. The Burgers vector of this edge component, $\mathbf{b}_z^e$, which is parallel to the nanowire axis (*i.e.*, the *c*-axis), is also quantized in multiples of the interlayer spacing of the layered crystal (Figure S1). If the overall Burgers vector

$\mathbf{b}_z$ remains constant during the climb, $\mathbf{b}_z^s$ is reduced compared to the Burgers vector of the original screw dislocation, so that $\mathbf{b}_z = \mathbf{b}_z^s + \mathbf{b}_z^e$. All analyzed nanowires show similarly good agreement between predicted and observed twist, albeit in some cases for $\mathbf{b}_z^s = 1.04$ nm (*i.e.*, $\mathbf{b}_z > 1.04$ nm, see Table S1), demonstrating that the twist of helical dislocations in nanowires closely follows Eshelby's predictions. In addition to their reduced twist, diffraction patterns of layered nanowires with helical dislocations show other differences compared to wires with screw dislocations, for example a combined twist of the (*a*, *b*) crystal axes and tilt of the *c*- axis along the nanowire replacing the simple twist caused by screw dislocations (Figure S7; Movies S1, S2).

Control over single helical dislocations via the core-shell c-axis mismatch

Helical dislocations are generated by climb of a dislocation with pure screw character in the presence of excess vacancies.[45] In pure GeS nanowires no helices are found, which supports the conclusion that core-shell mismatch is the main driver of the formation of helical dislocations. The advantage of using misfit stress – here generated in $Ge_{1-x}Sn_xS$ core-shell wires – to produce helical dislocations lies in the inherent ability to tune the geometry of the dislocation line (and hence the ratio between screw- and edge character of the mixed dislocation) *via* the core and shell composition, *i.e.*, the *c*-axis mismatch. The realization of such control over helical dislocations by tuning the nanowire composition is demonstrated in **Figure 3**, which shows TEM images of nanowires from different growth runs (see Table S2) with progressively increasing Sn content of the shell, starting from zero (pure GeS, Figure 3a) up to a maximum of ~35 at. % ($Ge_{0.3}Sn_{0.7}S$, Figure 3d). Corresponding Raman spectra documenting the mode shifts due to the increasing shell Sn content are shown in Figure S8. The evolution of the helical dislocation geometry is evident in TEM images (Figure 3a-d) as well as a statistical analysis of the

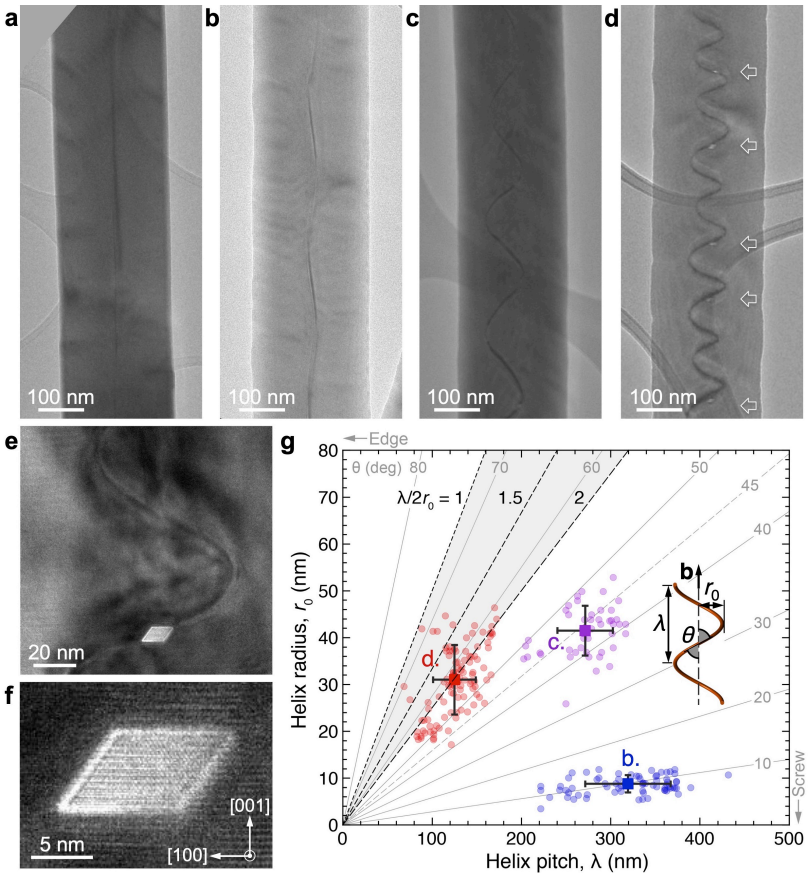

Figure 3. Control over helical dislocations in nanowires. a. – d. TEM images of $Ge_{1-x}Sn_xS$ nanowires with increasing Sn content, *x*, showing the transition from a straight screw dislocation (a.) to helical dislocations with progressively increasing amplitude and decreasing pitch (b.–d.). **e.** High-resolution TEM of one of the faceted voids along the helical dislocation (arrows in d.). **f.** Higher magnification of the Kirkendall void. **g.** Statistical analysis of the geometry (radius r_0, pitch λ, see inset) of helical dislocations in several nanowires, using TEM image data for samples with the three Sn concentrations represented in panels b.–d. Large symbols and error bars reflect the mean value and confidence intervals of plus and minus one standard deviation of the different data sets, respectively. Dashed lines and the shaded area delineate the predicted range of the equilibrium ratio between pitch λ and diameter $2r_0$ of a helical dislocation without external forces that is free to glide along its tangent cylinder.[32] Gray isolines mark the different angles θ between the dislocation line direction and the Burgers vector, where $\theta = 0°$ corresponds to a pure screw dislocation and $\theta = 90°$ to a pure edge dislocation.

distribution of helix radius (r_0) and pitch (λ) for the different shell compositions (Figure 3g). Pure GeS nanowires host straight axial screw dislocations (Figure 3a). For nanowires with helical dislocations, we find that the dislocation geometry follows a universal guiding principle: radius and pitch of the helix can vary as long as the edge/screw ratio of the Burgers vector ($|\mathbf{b}_z^e|/|\mathbf{b}_z^s| = \tan\theta$, where θ is the angle between the overall Burgers vector $\mathbf{b}_z$ and the helical dislocation line, see Figure S9) is preserved. In core-shell wires with low (shell) Sn content (*i.e.*, small core-shell

mismatch, Figure 3b), r_0 remains small (close to the straight line of the incipient screw dislocation) and shows little variation, while the pitch varies strongly. The origin of this behavior can be seen in Figure 3g. The measured (r_0, λ) distribution in this sample closely traces the isoline of constant angle $\theta \approx 10°$ between the Burgers vector and the dislocation line. Hence, the helix adopts a fixed $b_z^e/b_z^s \approx 1/5.7$, which can be fulfilled for a wide span of the pitch λ, but only a narrow range of helix radii r_0. Increasing the core-shell mismatch through a higher Sn content of the shell (Figure 3c) brings the edge/screw ratio to ~1/1 (Figure 3g). The measured (r_0, λ) values again follow the corresponding isoline ($\theta \approx 45°$), which in this case implies a narrow spread of both radius and pitch of the helix. Nanowires with the largest core-shell mismatch realized here (Figure 3d) reach $b_z^e/b_z^s \approx 1.7/1$ (Figure 3g). In this regime, tracing the corresponding isoline ($\theta \approx 60°$) implies a narrowly defined pitch λ but allows large variations in radius r_0, as observed for the helical dislocations in this sample. At this stage, the geometry of the helical dislocation approaches the predicted ratio between the pitch λ and diameter $2r_0$ in equilibrium,[32] with $\lambda/2r_0 \approx 2$. Finally, for wires with large core-shell mismatch, TEM shows arrays of faceted voids[51] decorating the helical dislocation (Figure 3d-f). This observation confirms the presence of excess thermal vacancies at the growth temperature (coalesced into faceted vacancy clusters/voids during cooling) that are required for the formation of helical dislocations by climb of the incipient screw dislocation.[45]

Optoelectronic signatures of the transition from axial screw to helical dislocations

In 3D semiconductors, screw dislocations were found to be relatively benign in carrier transport and recombination[4] while edge dislocations give rise to deep-level nonradiative recombination centers in the gap.[5, 52] These differences suggest the ability of tracking electronic structure modifications due to the transition from an axial screw to a helical dislocations *via*

optoelectronic measurements, here single-nanowire cathodoluminescence (CL) excited by the focused electron beam in STEM. To detect the introduction of gap states by the edge component of helical dislocations, we analyzed the competition between radiative and nonradiative recombination in GeS nanowires and $Ge_{1-x}Sn_xS$ core-shell wires *via* the spontaneous emission quantum efficiency probed by beam current dependent CL (**Figure 4**).[53]

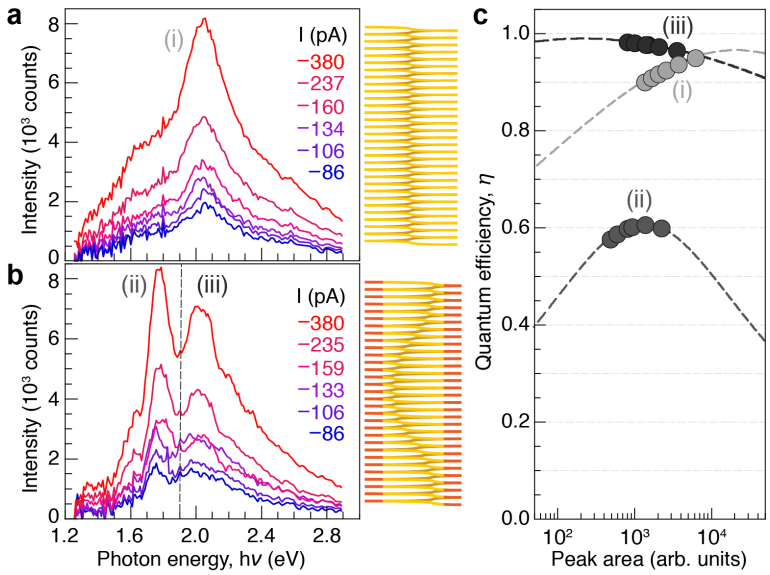

Figure 4. Electron beam current dependent STEM-CL. a. Current-dependent CL spectra of a GeS van der Waals nanowire containing a single axial screw dislocation, for beam currents ranging between 86 pA and 380 pA. **b.** Current-dependent CL spectra of a $Ge_{1-x}Sn_xS$ alloy core-shell nanowire hosting a helical dislocation with $b_z^e/b_z^s \approx 1/1$ ($\theta \approx 45°$, see Figure 3c). **c.** Analysis of the spontaneous emission quantum efficiency (η) of the GeS nanowire (i), and for the band-edge peak (hv ≤ 1.9 eV) and the high-energy peak (hv ≥ 1.9 eV) of the $Ge_{1-x}Sn_xS$ nanowire.

Characteristic CL spectra of GeS nanowires containing a single axial screw dislocation show a dominant band-edge peak along with a shoulder to lower energy (Figure 4a). $Ge_{1-x}Sn_xS$ core-shell nanowires hosting helical dislocations with edge/screw ratio ~1 show a modified spectrum with two distinct peaks (Figure 4b), possibly due to separate contributions from the core and shell materials or as a result of a nonradiative recombination channel producing a spectral region (here centered at ~1.9 eV) with quenched light emission, similar to previous findings for GeS ribbons with twin defects.[53] The latter explanation is supported by additional CL experiments.

Electron beam current dependent CL spectra were analyzed by fitting with three components, corresponding to radiative, nonradiative (Shockley-Read-Hall), and Auger recombination (Figure S10), from which the spontaneous emission quantum efficiency η was derived (Figure 4c). GeS nanowires with axial screw dislocations show a high quantum efficiency $\eta > 0.9$ at room temperature. In $Ge_{1-x}Sn_xS$ core-shell nanowires, a more complex behavior is observed. For the low-energy region (including the band-edge peak centered at ~1.7 eV), η drops to 0.6, indicating the opening of a nonradiative recombination channel that competes with radiative recombination for band-edge electron-hole pairs. This behavior is consistent with the introduction of gap states by the edge component of the helical dislocation, analogous to 3D semiconductors.[5, 52] The higher-energy region (including the peak at ~2.1 eV), on the other hand, shows predominant radiative recombination with near-unity quantum efficiency, indicative of an above-bandgap transition with fast radiative recombination. The identification of other effects on the optoelectronic properties, *e.g.*, associated with different Burgers vectors $\mathbf{b}_z$ of the helical dislocations (see Table S1), will require additional work beyond the scope of this study.

3. Conclusions

Our results show that van der Waals nanowires afford unprecedented control over dislocations, facilitated by the disposition of layered crystals toward forming out-of-plane growth spirals and a reduced set of possible Burgers vectors perpendicular to the layer plane (in contrast to nanowires of 3D crystals, such as PbS or ZnO, whose crystallography supports a wider range of Burgers vectors and which can therefore form pure screw[51] or mixed dislocations).[40] A large majority of GeS nanowires obtained by VLS processes host one axial screw dislocation per wire, which can be caused to exit by suitable thermal protocols.[41] In core-shell van der Waals nanowires, such axial screw dislocations are rationally transformed into mixed helical

dislocations whose geometry (radius, pitch) and hence ratio of screw- and edge Burgers vector components is tunable *via* the core-shell *c*-axis mismatch. While we demonstrated this tuning of individual mixed dislocations in $Ge_{1-x}Sn_xS$ alloy core-shell nanowires formed by spontaneous phase separation in a single-step VLS process, one can envision alternative synthesis strategies such as the sequential growth of the nanowire core and shell from materials that provide a tunable axial lattice mismatch. The nanowire geometry plays an important role in facilitating dislocation control, through the stable positioning of incipient screw dislocations on the wire axis[50] and by enabling dislocation mixing driven by the lattice mismatch in a core-shell geometry. Nanowires also provide a small-volume host matrix where emerging dislocation-induced phenomena can dominate the overall properties. It may be possible to extend our strategy for dislocation tuning – based on a core-shell geometry with variable axial mismatch between core and shell – to non-layered nanowires, provided that a core material that tends to form axial screw dislocations is integrated with a shell with the required axial lattice mismatch, and subject to the defect configurations allowed by the 3D crystal structure. The ability to position individual tunable dislocations in nanowires opens up unique opportunities for investigating the electronic, optoelectronic, and topological effects of dislocations, *e.g.*, by single nanowire charge or spin transport,[54] luminescence spectroscopy,[13] *etc*.

Experimental Section

Synthesis of $Ge_{1-x}Sn_xS$ nanowires: $Ge_{1-x}Sn_xS$ nanowires were synthesized by vapor-liquid-solid (VLS) growth involving simultaneous vapor transport from two powder precursors, GeS (99.99%, Sigma Aldrich) and SnS (99.99%, Sigma Aldrich), in a pumped two-zone quartz tube reactor. The substrates were Si(100) wafers covered by sputtering with thin (2-4 nm) Au films, which dewetted at the growth temperature. The first (upstream) zone of the reactor containing SnS powder (50 mg) in a quartz boat was heated to 650-670°C while a second quartz boat with GeS powder (20 mg), located outside the first zone, was heated to ~430-450°C. These conditions yield vapor pressures of ~250 mTorr for GeS (at 450°C)[43] and ~100 mTorr for SnS (at 670°C).[43] The sample was held in the second (downstream) temperature-controlled zone heated to 275-

285°C. During growth, the quartz reactor was pumped by a mechanical pump and a carrier gas (Ar, 99.9999%) flow was maintained at 60 standard cubic centimeters per minute (sccm) at a pressure of 20 mTorr. The reactor temperatures were ramped so that the above temperature settings were reached simultaneously and held for a growth time of 5 minutes, followed by natural cooling to room temperature. The growth resulted in the formation of nanowires with lengths of several tens of micrometers. For the preparation of control samples of pure GeS nanowires, only the crucible containing GeS was introduced in the system and the nanowires were grown at substrate temperature of 300°C.[13]

Electron microscopy and nanobeam electron diffraction: Structure and morphology of the nanowires were investigated by (scanning) transmission electron microscopy ((S)TEM) imaging and nanobeam diffraction in an FEI Talos F200X microscope at 200 kV. For all (S)TEM experiments, the as-grown nanowires were dry-transferred to lacey carbon supports.

Energy dispersive X-ray spectroscopy (EDS) in STEM: STEM-EDS maps (1024×1024 pixels) and EDS line scans (13 nm step size) were collected using a JEOL NeoARM S/TEM operating at 80 kV.

Single nanowire STEM cathodoluminescence (CL): Cathodoluminescence spectroscopy was performed in STEM mode (STEM-CL) using a Gatan Vulcan CL holder at room temperature, 200 keV electron energy and incident electron beam currents ranging from 86 pA to 380 pA. Hyperspectral linescans were acquired by displacing the focused electron beam in predefined equal steps across single nanowires and acquiring full CL spectra (integration time: 10 s per spectrum) at each beam position. CL spectra were obtained using a 300 mm Czerny-Turner spectrometer and a thermoelectric-cooled back-illuminated Si CCD detector (1340 × 100 array). The spectra shown in Figure 4 represent averages of 6 individual spectra extracted from linescans across the corresponding nanowires, obtained within ± 9 nm around the centerline of the wires.

Micro-Raman spectroscopy: Micro-Raman spectroscopy and Raman linescans were measured on individual nanowires dry-transferred to SiN_x membrane chips (Norcada) using a Raman microscope (Horiba Xplora plus) with an excitation wavelength of 532 nm, 100× objective (lateral resolution ~0.5 μm), 16.8 μW laser power, and a 2400 lines/mm grating.

Acknowledgements. This work was supported by the National Science Foundation, Division of Materials Research, Solid State and Materials Chemistry Program under Grant No. DMR-1904843. STEM-EDS measurements were supported by the Center for Nanophase Materials Sciences (CNMS), which is a US Department of Energy, Office of Science User Facility at Oak Ridge National Laboratory.

Funding:

National Science Foundation Grant No. DMR-1904843 (PS, ES)

U.S. Department of Energy, Office of Science contract No. DE-AC05-00OR22725 (RRU, through CNMS/ORNL).

Supporting Information: Supporting Figures: Dislocations in 2D and van der Waals crystals; electron microscopy and diffraction of nanowires with screw- and helical dislocations; Eshelby twist in filled & hollow rods with screw dislocations, compared to helical dislocations; Raman spectroscopy of $Ge_{1-x}Sn_xS$ alloy core-shell nanowires; screw- and edge component of helical dislocations; analysis of electron beam-current dependent CL spectra. Supporting Movies: Nanobeam electron diffraction along nanowires with screw- and mixed/helical dislocations. Supporting Tables: Eshelby twist analysis; growth conditions of nanowires with helical dislocations. (PDF)

Conflict of Interest: The authors declare no competing financial interest.

References

1. Freysoldt, C.; Grabowski, B.; Hickel, T.; Neugebauer, J.; Kresse, G.; Janotti, A.; Van de Walle, C. G., First-principles calculations for point defects in solids. *Reviews of Modern Physics* **2014,** *86*, 253-305.
2. Mott, N. F., Electrons in disordered structures. *Advances in Physics* **1967,** *16*, 49-144.
3. Figielski, T., Recombination at dislocations. *Solid-State Electronics* **1978,** *21*, 1403-1412.
4. Collins, C. V.; Miles, M. H., Electrical Effects of Screw Dislocations in Germanium. *Journal of Applied Physics* **1971,** *42*, 5644-5648.
5. Miles, M. H., Extrinsic Photoconductivity from Edge Dislocations in Germanium. *Journal of Applied Physics* **1969,** *40*, 2720-2724.
6. Chynoweth, A. G.; Pearson, G. L., Effect of Dislocations on Breakdown in Silicon p-n Junctions. *Journal of Applied Physics* **1958,** *29*, 1103-1110.
7. Sze, S. M.; Ng, K. K., Physics and Properties of Semiconductors—A Review. In *Physics of Semiconductor Devices*, Wiley: Hoboken (NJ), 2006; pp 5-75.
8. Balasubramanian, G.; Neumann, P.; Twitchen, D.; Markham, M.; Kolesov, R.; Mizuochi, N.; Isoya, J.; Achard, J.; Beck, J.; Tissler, J.; Jacques, V.; Hemmer, P. R.; Jelezko, F.; Wrachtrup, J., Ultralong spin coherence time in isotopically engineered diamond. *Nature Materials* **2009,** *8*, 383-387.
9. Zhang, G.; Cheng, Y.; Chou, J.-P.; Gali, A., Material platforms for defect qubits and single-photon emitters. *Applied Physics Reviews* **2020,** *7*, 031308.
10. Chabanon, M.; Rangamani, P., Geometric coupling of helicoidal ramps and curvature-inducing proteins in organelle membranes. *Journal of The Royal Society Interface* **2019,** *16*, 20190354.
11. Terasaki, M.; Shemesh, T.; Kasthuri, N.; Klemm, Robin W.; Schalek, R.; Hayworth, Kenneth J.; Hand, Arthur R.; Yankova, M.; Huber, G.; Lichtman, Jeff W.; Rapoport, Tom A.; Kozlov, Michael M., Stacked Endoplasmic Reticulum Sheets Are Connected by Helicoidal Membrane Motifs. *Cell* **2013,** *154*, 285-296.
12. Frank, F. C., The influence of dislocations on crystal growth. *Discussions of the Faraday Society* **1949,** *5*, 48-54.
13. Sutter, P.; Wimer, S.; Sutter, E., Chiral twisted van der Waals nanowires. *Nature* **2019,** *570*, 354-357.

14. Hu, L.; Huang, H.; Wang, Z.; Jiang, W.; Ni, X.; Zhou, Y.; Zielasek, V.; Lagally, M. G.; Huang, B.; Liu, F., Ubiquitous Spin-Orbit Coupling in a Screw Dislocation with High Spin Coherency. *Physical Review Letters* **2018,** *121*, 066401.
15. Rex, S.; Willa, R., A topological flux trap: Majorana bound states at screw dislocations. *New Journal of Physics* **2022,** *24*, 053057.
16. Chernodub, M. N.; Zubkov, M. A., Chiral anomaly in Dirac semimetals due to dislocations. *Physical Review B* **2017,** *95*, 115410.
17. Sumiyoshi, H.; Fujimoto, S., Torsional Chiral Magnetic Effect in a Weyl Semimetal with a Topological Defect. *Physical Review Letters* **2016,** *116*, 166601.
18. Soto-Garrido, R.; Muñoz, E.; Juričić, V., Dislocation defect as a bulk probe of monopole charge of multi-Weyl semimetals. *Physical Review Research* **2020,** *2*, 012043.
19. Ran, Y.; Zhang, Y.; Vishwanath, A., One-dimensional topologically protected modes in topological insulators with lattice dislocations. *Nature Physics* **2009,** *5*, 298-303.
20. Li, M.; Tsurimaki, Y.; Meng, Q.; Andrejevic, N.; Zhu, Y.; Mahan, G. D.; Chen, G., Theory of electron–phonon–dislon interacting system—toward a quantized theory of dislocations. *New Journal of Physics* **2018,** *20*, 023010.
21. Li, M., Quantized dislocations. *Journal of Physics: Condensed Matter* **2019,** *31*, 083001.
22. Fu, C.-L.; Li, M., Oscillatory deviations from Matthiessen's rule due to interacting dislocations. *Journal of Physics: Condensed Matter* **2017,** *29*, 325702.
23. Hu, S.; Zhang, H.; Xiong, S.; Zhang, H.; Wang, H.; Chen, Y.; Volz, S.; Ni, Y., Screw dislocation induced phonon transport suppression in SiGe superlattices. *Physical Review B* **2019,** *100*, 075432.
24. Fogel, N. Y.; Pokhila, A. S.; Bomze, Y. V.; Sipatov, A. Y.; Fedorenko, A. I.; Shekhter, R. I., Novel Superconducting Semiconducting Superlattices: Dislocation-Induced Superconductivity? *Physical Review Letters* **2001,** *86*, 512-515.
25. Medvedev, O.; Vyvenko, O.; Ubyivovk, E.; Shapenkov, S.; Bondarenko, A.; Saring, P.; Seibt, M., Intrinsic luminescence and core structure of freshly introduced a-screw dislocations in n-GaN. *Journal of Applied Physics* **2018,** *123*, 161427.
26. Reiche, M.; Kittler, M.; Erfurth, W.; Pippel, E.; Sklarek, K.; Blumtritt, H.; Haehnel, A.; Uebensee, H., On the electronic properties of a single dislocation. *Journal of Applied Physics* **2014,** *115*, 194303.
27. Zhang, L.; Liu, K.; Wong, A. B.; Kim, J.; Hong, X.; Liu, C.; Cao, T.; Louie, S. G.; Wang, F.; Yang, P., Three-Dimensional Spirals of Atomic Layered MoS2. *Nano Letters* **2014,** *14*, 6418-6423.
28. Shearer, M. J.; Samad, L.; Zhang, Y.; Zhao, Y.; Puretzky, A.; Eliceiri, K. W.; Wright, J. C.; Hamers, R. J.; Jin, S., Complex and Noncentrosymmetric Stacking of Layered Metal Dichalcogenide Materials Created by Screw Dislocations. *Journal of the American Chemical Society* **2017,** *139*, 3496-3504.
29. Yazyev, O. V.; Louie, S. G., Topological defects in graphene: Dislocations and grain boundaries. *Physical Review B* **2010,** *81*, 195420.
30. Seitz, F., The Generation of Vacancies by Dislocations. *Physical Review* **1950,** *79*, 1002-1003.
31. Weertman, J., Helical Dislocations. *Physical Review* **1957,** *107*, 1259-1261.
32. Veyssiere, P.; Grilhe, J., Experimental study of the influence of some parameters on the helical dislocations equilibrium in quenched alloys. *Acta Metallurgica* **1971,** *19*, 1047-1051.

33. Horibuchi, K.; Yamaguchi, S.; Kimoto, Y.; Nishikawa, K.; Kachi, T., Formation of helical dislocations in ammonothermal GaN substrate by heat treatment. *Semiconductor Science and Technology* **2016,** *31*, 034002.
34. Amelinckx, S.; Bontinck, W.; Maenhout-Van der Vorst, W., Helical dislocations in GaF2 and NaCl crystals. *Physica* **1957,** *23*, 270-272.
35. Amelinckx, S.; Bontinck, W.; Dekeyser, W.; Seitz, F., On the formation and properties of helical dislocations. *Philosophical Magazine* **1957,** *2*, 355-378.
36. Jones, D. A.; Mitchell, J. W., Observations on helical dislocations in crystals of silver chloride. *The Philosophical Magazine: A Journal of Theoretical Experimental and Applied Physics* **1958,** *3*, 1-7.
37. Thomas, G.; Whelan, M. J., Helical dislocations in quenched aluminium-4% copper alloys. *The Philosophical Magazine: A Journal of Theoretical Experimental and Applied Physics* **1959,** *4*, 511-527.
38. Haley, J. C.; Liu, F.; Tarleton, E.; Cocks, A. C. F.; Odette, G. R.; Lozano-Perez, S.; Roberts, S. G., Helical dislocations: Observation of vacancy defect bias of screw dislocations in neutron irradiated Fe–9Cr. *Acta Materialia* **2019,** *181*, 173-184.
39. Wagner, G.; Gottschalch, V., Helical dislocations in Sn-doped GaP epitaxial layers and their characterization by transmission electron microscopy. *Philosophical Magazine A* **1985,** *52*, 395-406.
40. Bierman, M. J.; Lau, Y. K. A.; Kvit, A. V.; Schmitt, A. L.; Jin, S., Dislocation-Driven Nanowire Growth and Eshelby Twist. *Science* **2008,** *320*, 1060-1063.
41. Sutter, P.; Idrobo, J.-C.; Sutter, E., Van der Waals Nanowires with Continuously Variable Interlayer Twist and Twist Homojunctions. *Advanced Functional Materials* **2021,** *31*, 2006412.
42. Sutter, E.; Sutter, P., Ultrathin Twisted Germanium Sulfide van der Waals Nanowires by Bismuth Catalyzed Vapor–Liquid–Solid Growth. *Small* **2021,** *17*, 2104784.
43. Mills, K. C., *Thermodynamic Data for Inorganic Sulphides, Selenides and Tellurides*. Butterworths: London, 1974; p 328-332.
44. Sutter, E.; French, J. S.; Sutter, P., Tunable Layer Orientation and Morphology in Vapor–Liquid–Solid Growth of One-Dimensional GeS van der Waals Nanostructures. *Chemistry of Materials* **2021,** *33*, 3980-3988.
45. Amelinckx, S., Dislocations in ionic crystals. *Il Nuovo Cimento (1955-1965)* **1958,** *7*, 569-599.
46. Predel, B. *Ge - Sn (Germanium - Tin): Datasheet from Landolt-Börnstein - Group IV Physical Chemistry · Volume 12C: "Dy - Er ... Ir - Y" in SpringerMaterials*, Springer-Verlag Berlin Heidelberg: 2013.
47. Sutter, P.; French, J. S.; Khosravi Khorashad, L.; Argyropoulos, C.; Sutter, E., Optoelectronics and Nanophotonics of Vapor–Liquid–Solid Grown GaSe van der Waals Nanoribbons. *Nano Letters* **2021,** *21*, 4335-4342.
48. Zhu, J.; Peng, H.; Marshall, A. F.; Barnett, D. M.; Nix, W. D.; Cui, Y., Formation of chiral branched nanowires by the Eshelby Twist. *Nature Nanotechnology* **2008,** *3*, 477-481.
49. Eshelby, J. D., The distortion and electrification of plates and rods by dislocations. *Physica Status Solidi B-basic Solid State Physics* **1962,** *2*, 1021-1028.
50. Eshelby, J. D., Screw Dislocations in Thin Rods. *Journal of Applied Physics* **1953,** *24*, 176-179.

51. Morin, S. A.; Bierman, M. J.; Tong, J.; Jin, S., Mechanism and Kinetics of Spontaneous Nanotube Growth Driven by Screw Dislocations. *Science* **2010,** *328*, 476-480.
52. Jastrzębska, M.; Figielski, T., Trapping Processes at Dislocations in Plastically Bent Germanium. *Physica Status Solidi (b)* **1966,** *14*, 381-390.
53. Sutter, E.; French, J. S.; Komsa, H.-P.; Sutter, P., 1D Germanium Sulfide van der Waals Bicrystals by Vapor–Liquid–Solid Growth. *ACS Nano* **2022,** *16*, 3735-3743.
54. van 't Erve, O. M. J.; Friedman, A. L.; Li, C. H.; Robinson, J. T.; Connell, J.; Lauhon, L. J.; Jonker, B. T., Spin transport and Hanle effect in silicon nanowires using graphene tunnel barriers. *Nature Communications* **2015,** *6*, 7541.

Table of Contents Graphic